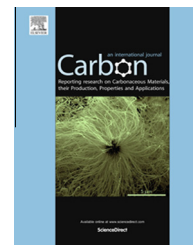


Available at www.sciencedirect.com

ScienceDirect

journal homepage: www.elsevier.com/locate/carbon

Solvent-free mechanochemical reduction of graphene oxide

Dong Wook Chang ^{a,1}, Hyun-Jung Choi ^{b,1}, In-Yup Jeon ^b, Jeong-Min Seo ^b, Liming Dai ^{c,*}, Jong-Beom Baek ^{b,*}

^a Department of Chemical Systematic Engineering, Catholic University of Daegu, 13-13, Hayang, Gyeongbuk 712-702, South Korea

^b School of Energy and Chemical Engineering/Low-Dimensional Carbon Materials Center, Ulsan National Institute of Science and Technology (UNIST), 100, Banyeon, Ulsan 689-798, South Korea

^c Department of Macromolecular Science and Engineering, Case Western Reserve University, Cleveland, OH 44106, USA

ARTICLE INFO

Article history:

Received 22 February 2014

Accepted 21 May 2014

Available online 2 June 2014

ABSTRACT

We report a versatile and eco-friendly approach for the reduction of graphene oxide into high-quality graphene nanoplatelets by simple solid-state mechanochemical ball-milling in the presence of hydrogen. After the ball-milling process, the resultant graphene nanoplatelets show the efficient restoration of the graphitic structure completely free from any heteroatom doping (e.g., nitrogen, sulfur) and enhanced electrical conductivities up to 120 and 3400 S/m before and after an appropriate heat treatment (e.g., 900 °C for 2 h under nitrogen).

© 2014 Elsevier Ltd. All rights reserved.

1. Introduction

Along with the recent explosive interest on graphene due to its outstanding mechanical, thermal and electrical properties [1–3], several synthesis methods have been developed to prepare graphene nanoplatelets (GnPs), including a simple mechanical exfoliation from graphite [4], chemical vapor deposition (CVD) [5], solvothermal synthesis [6], epitaxial growth [7], and graphitization of graphene oxide (GO) [8,9]. Among them, the chemical reduction of GO into reduced graphene oxide (RGO) has been the most widely investigated approach to GnPs with a good processability and scalability [1,8–10]. However, the preparation of RGO often involves the use of very toxic and hazardous reducing agents, such as hydrazine [9,11] and NaBH₄ [12,13]. In addition, the undesirable incorporation of heteroatoms from the reducing agent (e.g., nitrogen from hydrazine) into graphene network could

significantly alter the electronic properties of GnPs produced by chemical reduction [9,14,15]. To address the aforementioned issues, several alternative approaches for the transformation of GO into RGO have been reported, including the reduction of GO by biomolecules as reducing agents [16–20], irradiations (e.g., laser [21,22], UV [23,24]), electrochemical method [25], and thermal treatments [26–28]. Like all other methods for reducing GO to RGO, however, these green reduction methods of GO are still suffered from an incompleting reduction, and hence a non-integrated graphitic network in the final products.

Recently, we have developed a simple, but efficient, approach to the large-scale production of edge-functionalized graphene nanoplatelets (EFGnPs) with minimal basal plane distortion by mechanochemical ball-milling of graphite [29,30]. The EFGnPs display promising properties, including high electrical conductivity and outstanding electrocatalytic

* Corresponding authors: Fax: +82 52 217 2019.

E-mail addresses: liming.dai@case.edu (L. Dai), jbbaek@unist.ac.kr (J.-B. Baek).

¹ These authors contributed equally to this work.

<http://dx.doi.org/10.1016/j.carbon.2014.05.055>

0008-6223/© 2014 Elsevier Ltd. All rights reserved.

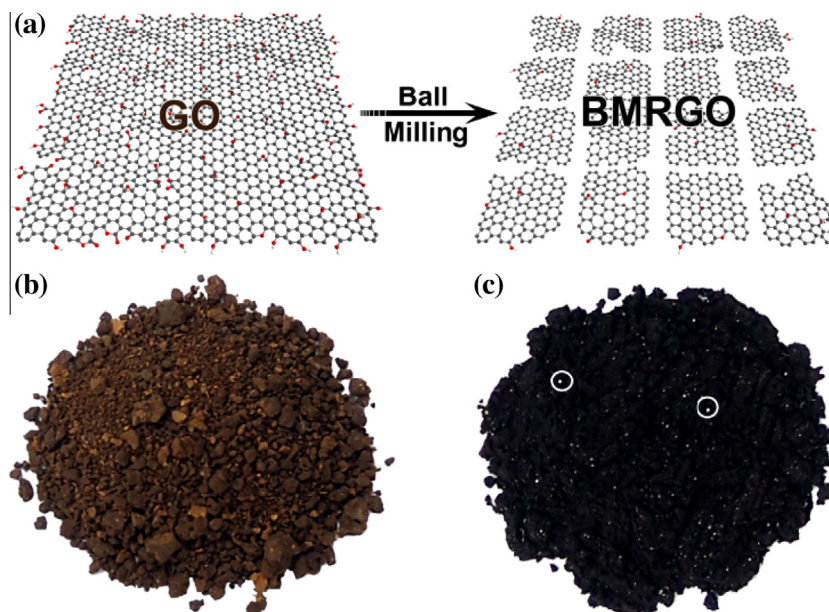


Fig. 1 – (a) A schematic representation of solvent-free mechanochemical reduction of graphene oxide (GO) in the presence of hydrogen. Photographs: (b) GO; (c) BMRGO. The color change from GO (brown) to BMRGO30 (dark black) is a visual indication of the mechanochemical reduction and the shiny light reflection (white circles) of BMRGO30 implies high crystallinity. (A colour version of this figure can be viewed online.)

activity toward oxygen reduction reaction (ORR) [31,32]. By ball-milling of graphite with different reactants, various chemically functionalized GnPs were produced [33–35].

To avoid the solution-based reduction process with multiple drawbacks (*vide supra*), we report here a simple method for eco-friendly, solid-state mechanochemical reduction of GO into GnPs by ball-milling of GO, instead of pristine graphite used for our previous reports [29–32], in the presence of hydrogen (Fig. 1). We found that the ball-milled reduced graphene oxide (BMRGO) pellets with an efficiently-restored graphitic structure free from any heteroatom doping exhibited electrical conductivities up to 120 and 3400 S/m before and after an appropriate heat treatment (e.g., 900 °C for 2 h under nitrogen, *vide infra*), respectively. Therefore, the solid-state ball-milling approach, involving no hazardous chemicals to generate undesirable contaminant(s), outperforms the commonly used solution-based reduction process for mass production of high-quality GnPs.

2. Experimental section

2.1. Materials and preparation of ball-milled reduced graphene (BMRGO)

Graphite (Alfar Aesar, natural graphite, 100 mesh, 99.9995% metal basis, Lot#F22U001) was used as the starting material in this study. Firstly, GO was prepared by the modified Hummers' method from graphite [36]. The ball-milling of GO to produce ball-milled reduced graphene oxide (BMRGO) was carried out in a planetary micro ball-mill machine (Pulverisette 7 premium line, Fritsch) at 900 rpm. In a typical experiment, 2.0 g of GO and hydrogen gas (10 bar, Daesung Industrial Gases Co., Ltd.) were charged into a stainless steel

capsule containing stainless steel balls of 5 mm in diameter. The container was fixed in a planetary ball-mill machine and rotated at 900 rpm for a operation time ranging from 30 to 240 min to produce various ball-milled reduced graphene oxides (BMRGO), including BMRGO30, BMRGO60, BMRGO120, BMRGO180 and BMRGO240 (the digital number refers to 30, 60, 120, 180 and 240 min, respectively). After opening the container lid at the end of ball-milling, the resultant black powders were carefully collected and purified by Soxhlet extraction with a 1 M HCl solution to remove metallic impurities. The purified powders were washed with a plenty of water and methanol and the final products were dried in vacuum oven at 80 °C under a reduced pressure for 48 h to yield 1.15 g of BMRGO30, 1.09 g of BMRGO60, 1.05 g of BMRGO120, 1.03 g of BMRGO180 and 1.01 g of BMRGO240, respectively.

2.2. Characterizations

Elemental analysis (EA) was conducted with a Thermo Scientific Flash 2000. The surface area was measured by nitrogen-adsorption-desorption isotherms using the Brunauer–Emmett–Teller (BET) method on Micromeritics ASAP 2504N. Thermogravimetric analysis (TGA) was conducted with a TA Q200 (TA Instrument) under air atmosphere at a heating rate of 10 °C min⁻¹. Solid-state ¹³C magic-angle spinning (MAS) NMR spectra were recorded on a Varian Unitynova 600 (600 MHz) spectrometer, using a 5-mm probe spinning at 9 kHz. Fourier transform infrared (FT-IR) spectra were recorded on a Perkin–Elmer Spectrum 100 using KBr pellets. Raman spectra were taken with a He–Ne laser (532 nm) as the excitation source by using confocal Raman microscopy (Alpha 300S, WITec, Germany), in conjunction with atomic force microscopy (AFM). X-ray diffraction (XRD) patterns were

recorded on a Rigaku D/MAZX 2500V/PC with Cu-K α radiation (35 kV, 20 mA, $\lambda = 1.5418 \text{ \AA}$). X-ray photoelectron spectra (XPS) were recorded on a Thermo Fisher K-alpha XPS spectrometer. The field emission scanning electron microscopy (FE-SEM) was performed with a FEI Nanonova 230, while the high-resolution transmission electron microscopy (HR-TEM) employed in this work is a JEOL JEM-2100F (Cs) microscope operating at 200 kV. The TEM specimens were prepared by dipping carbon micro-grids (Ted Pella Inc., 200 Mesh Copper Grid) into well-dispersed samples in NMP. UV–vis spectra were measured using Perkin–Elmer Lambda 35. Atomic force microscopy (AFM) analysis was conducted with Veeco Multimode V. The BMRGO pellets of diameter of 1.2 cm were prepared by compression molding at 3000 bar using hydraulic press (Specac Inc, Model No.: 21984). Conductivities of the BMRGO pellets were measured by four-point probe method (Advanced Instrument Technology (AIT) CMT-SR1000N). The sheet resistance of each sample was determined from average values of five measurements.

3. Results and discussion

Chemical compositions of all samples (i.e., graphite, GO, BMRGO30, BMRGO60, BMRGO120, BMRGO180 and BMRGO240) from the elemental analyses (EA) are summarized in Table S1. As expected, the pristine graphite is mainly composed of carbon atom (99.57 wt%). On the other hand, GO contains a large amount of oxygen (43.85 wt%) due to the generation of various oxygenated functional moieties, such as epoxy, hydroxyl, and carboxylic groups, by harsh oxidation during the modified Hummers' process [36,37]. Surprisingly, ball-milling induced dramatic decreases in oxygen contents for BMRGOs. It is noteworthy that these compositional changes from GO to BMRGOs are initially proportional to the ball-milling time up to 120 min, and then levelled-off at longer time (~ 240 min, Fig. 2a). For example, the carbon (C)/oxygen (O) ratio greatly increased from 1.51 for GO to 6.17 for BMRGO120 and finally reached to 6.80 for BMRGO240 (Fig. 2a), indicating an efficient solvent-free mechanochemical reduction of GO.

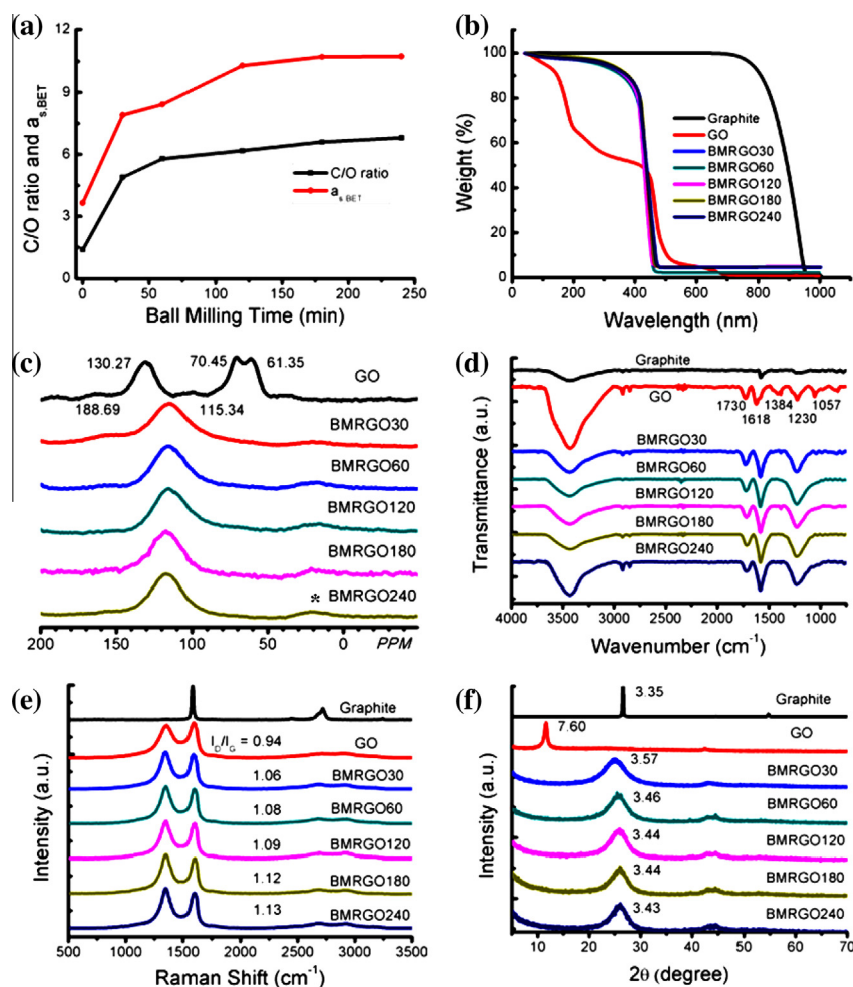


Fig. 2 – (a) Changes in C/O ratios based on EA and BET surface areas of samples with respect to ball-milling time; (b) TGA thermograms with heating rate of $10 \text{ }^\circ\text{C min}^{-1}$ in air; (c) Solid-state ¹³C magic-angle spinning (MAS) NMR spectra, * indicates the spinning sidebands [41,42]; (d) FT-IR spectra; (e) Raman spectra with I_D/I_G ratio; (f) XRD diffraction patterns and the numbers are d -spacing in angstrom (\AA) of graphite, GO, BMRGO30, BMRGO60, BMRGO120, BMRGO180 and BMRGO240. (A colour version of this figure can be viewed online.)

Interestingly, the Brunauer–Emmett–Teller (BET) surface area also marginally increased from 3.65 m²/g for GO to 10.30 m²/g for BMRGO120, and then levelled-off with further increasing ball-milling time (Fig. 2a). The BET results were well accordance with EA results (Table S1). The low surface areas of BMRGOs indicated that the efficient restoration of graphitic structure was occurred during ball-milling GO, implicating that kinetic energy (high speed balls) can be also used for the reduction of GO. Hence, mechanochemical ball-milling can reduce GO into RGO as well as grain size of RGO as precursor for delamination into a few layers upon dispersion in solvents (*vide infra*).

Thermogravimetric analyses (TGA) of all samples in air were conducted and the results are shown in Fig. 2b. As expected, GO shows a weight loss starting from 100 °C, attributable to the evaporation of bound water molecules between GO layers and from hygroscopic functional groups. The profound weight loss at around 200 °C is related to the eliminations of various oxygenated functional groups prior to the oxidative decomposition of the graphitic structure over 200–500 °C. Compared to GO, all BMRGOs show a greatly enhanced thermal stability due to the significant loss of oxygenated groups during ball-milling in the presence of hydrogen (Fig. 2b). Among BMRGOs, BMRGO30 shows the highest thermal stability due to its relatively large grain size.

The solid-state ¹³C magic-angle spinning (MAS) NMR measurements were also conducted to prove compositional changes of GO during ball-milling. As shown in Fig. 2c, GO exhibits several peaks at 61.35, 70.45, 188.69, and 130.37 ppm, arising from the ¹³C nuclei associated with epoxide group, hydroxyl group, carboxyl group, and unoxidized sp² carbons in the graphitic structure, respectively [9,12]. However, all BMRGOs display a major peak at around 115 ppm corresponding to the sp² carbon atoms, in which other oxygenated (61.35 and 70.45 ppm) and carbonyl (188.69 ppm) carbon peaks are overlapped due to the sensitivity of solid-state NMR measurements. These results reveal an efficient structural restoration of the graphitic structure (Fig. 2c) and are in accordance with the structural changes of GO during ball-milling (Fig. 1).

To further understand the structural changes before and after ball-milling, we carried out FT-IR spectroscopic measurements. As shown in Fig. 2d, GO displays several oxygenated peaks at 1730 (ν_{C=O}), 1618 (ν_{C=C}), 1384 (ν_{O-H}), 1230 (ν_{epoxy}) and 1057 cm⁻¹ (ν_{C-O}), along with hydroxyl bands (3400 cm⁻¹) in consistent with previous results [12,15,38]. However, all BMRGOs show a major characteristic peak at 1590 cm⁻¹ attributable to the in-plane vibration of sp² hybridized aromatic C=C in graphitic structure in conjunction with a concomitant decrease of several peaks from various oxygenated groups [18,19,39]. Once again, these results indicate that GO has been efficiently reduced during the mechanochemical ball-milling process.

Raman spectra obtained from all powder samples are shown in Fig. 2e. For the pristine graphite, the G and 2D bands are clearly observable at 1564 and 2679 cm⁻¹, respectively. In addition, the ratio of the D to G-band intensity (*I_D/I_G*) of the graphite approaches almost zero (~0.01) as the D band at 1335 cm⁻¹ associated with the edge distortion is negligible due to its large grain size. However, GO showed a broad and strong D band at 1357 cm⁻¹ with a relatively high *I_D/I_G* ratio

of 0.94, indicating an increased structural distortion and size reduction of the in-plane sp² domains. Furthermore, the G band of GO at 1598 cm⁻¹ is slightly up-shifted from that of graphite at 1564 cm⁻¹ due to the existence of isolated double bonds with higher resonance frequencies than that of the G band in graphite [40]. All BMRGOs show similar D and G bands at 1357 and 1598 cm⁻¹, respectively, but a gradually increased *I_D/I_G* ratio with increasing ball-milling time due to the grain size reduction during ball-milling [29].

The powder X-ray diffraction (XRD) patterns of all samples are shown in Fig. 2f. A sharp and strong peak at 2θ = 26.6° (*d*-spacing ~ 3.35 Å) was observed for the pristine graphite while a broad and weak peak at 2θ = 11.6° (*d*-spacing ~ 7.60 Å) was obtained from GO, indicating a lattice expansion by the oxygenated functional groups and “bound” small molecules between layers of GO. In comparison to GO, the XRD peaks for BMRGOs significantly shifted up to 2θ = 25.94° (*d*-spacing ~ 3.43 Å), indicating an efficient reduction of GO during ball-milling. This is consistent with the RGO produced by other solution-based environmental-friendly approaches [18,19], though the peaks from BMRGOs are somewhat sharper and narrower.

The chemical compositional changes during ball-milling of GO were further analyzed by X-ray photoelectron spectroscopy (XPS) (Fig. S2). Fig. 3 shows the high resolution C 1s XPS spectra of all samples investigated in this study. As expected, the pristine graphite displays a prominent peak at 284.3 eV from the graphitic sp² carbon. However, the high resolution C 1s peak of GO can be deconvoluted into several peaks at 284.3, 285.6 and 288.7 eV, corresponding to C=C, C-O and C=O, respectively (Fig. 3b) [9,26,41]. Upon ball-milling of GO in the presence of hydrogen, a dramatic decrease in the oxygen-bonded carbon components of the C 1s peak is observed (e.g., BMRGO30, Fig. 3c), revealing the efficient removal of the oxygenated functional groups in GO by ball-milling. Further diminution in intensities of the oxygen-bonded C 1s peaks is observed for other BMRGOs with a longer ball-milling time. These results indicate an efficient mechanochemical reduction of GO even in solid-state by ball-milling.

Comparing with GO, all BMRGOs display a significantly enhanced broad UV–vis absorbance with increasing the ball-milling time up to 900 nm (Fig. S3), indicating that the electronic conjugation within the graphitic structure is largely retained by the mechanochemical reduction during ball-milling of GO in the presence of hydrogen [23,28,41].

The morphological and micro-structural changes of GO during ball-milling were monitored by scanning electron microscopy (SEM) and transmission electron microscopy (TEM). As shown in Fig. 4, the pristine graphite and GO show micro-scale (100 mesh, <150 μm) irregular particle grains while BMRGOs show a significant reduction of the grain size nearly inversely proportional to the ball-milling time (Fig. 4). Fig. 5 depicts typical TEM images obtained from the BMRGO30. As can be seen, a wrinkled paper-like morphology characteristic of GnP is observed at a low magnification (Fig. 5a). The edge-on view at a high magnification shows the highly crystalline interior (Fig. 5b), indicating the occurrence of a high degree structural restoration during mechanochemical ball-milling. The corresponding selected area electron diffraction (SAED) pattern with a hexagonal symmetry given in Fig. 5c further supports the

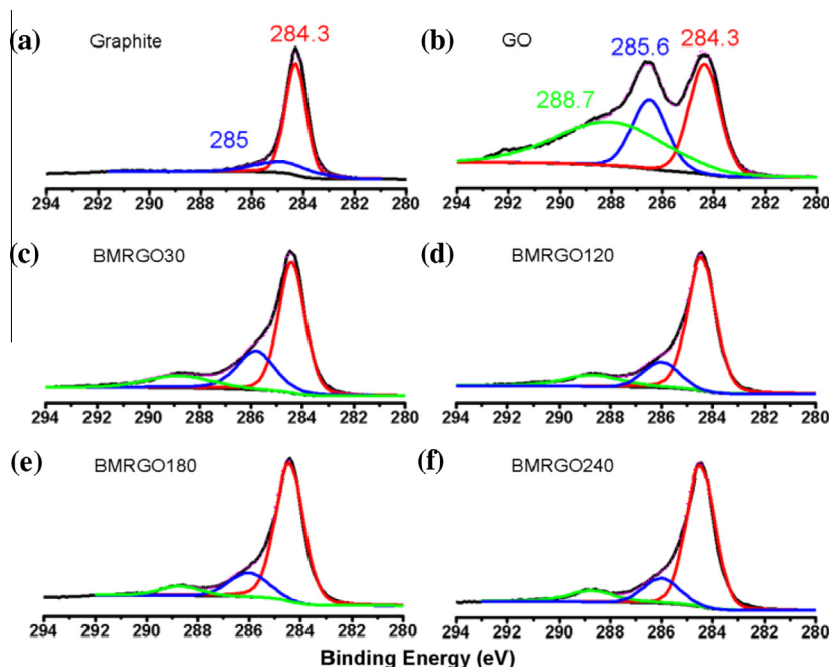


Fig. 3 – High resolution XPS C1s spectra: (a) graphite; (b) GO; (c) BMRGO30; (d) BMRGO120; (e) BMRGO180; (f) BMRGO240. (A colour version of this figure can be viewed online.)

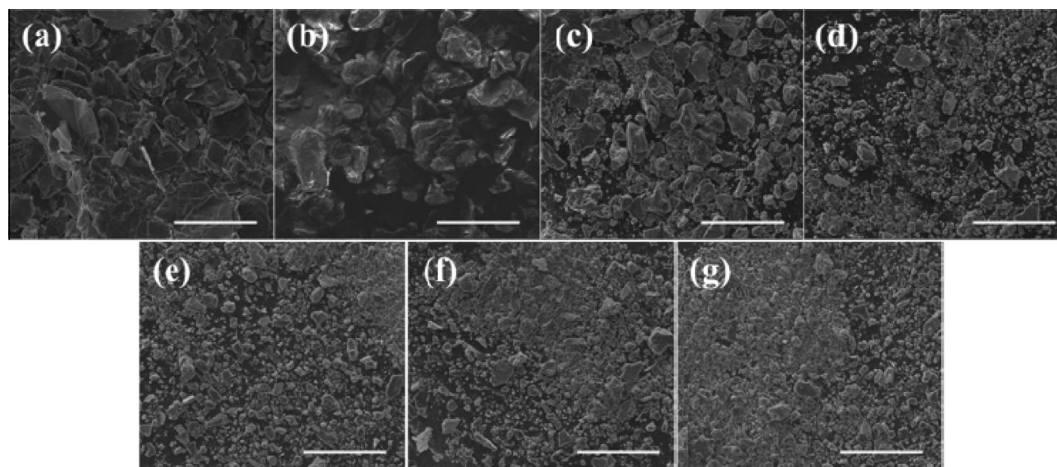


Fig. 4 – SEM images: (a) graphite, (b) GO, (c) BMRGO30, (d) BMRGO60, (e) BMRGO120, (f) BMRGO180 and (g) BMRGO240 at the same magnification. The scale bars are 100 μm .

high crystalline structure of BMRGO30, which is ascribed to a typical diffraction pattern of graphite [40,42]. Clearly, therefore, the graphitic structure has been well restored in BMRGOs. In addition, AFM analysis was also conducted to figure out the number of layers of BMRGOs. As shown in Fig. S4, BMRGO30 typically consisted of a few graphitic layers upon dispersion in solvents.

The four-probe van der Pauw method [29] was used to measure the electrical conductivity of all samples (GO and BMRGOs) for evaluation of the π -conjugated networks in the graphene structure. For the electrical measurements, powder samples of GO or BMRGOs were compressed into pellets with a diameter of 2.5 cm and thickness of approximately 200 μm

(Inset, Fig. 5d). Comparing with the electrical conductivity of GO (~ 0.2 S/m), the conductivity of BMRGOs increased as much as three orders of magnitude (in the range of 13–120 S/m), indicating an efficient structural restoration of π -conjugated networks in BMRGOs by removal of various oxygenated groups in GO during ball-milling. The highest conductivity of 120 S/cm is observed from BMRGO30, which decreased as the ball-milling time increased and finally reached to 13 S/m for BMRGO240 (Fig. 5c). The observed gradual decrease in conductivity from BMRGO30 to BMRGO240 is attributable to the reduction of grain size with increasing ball-milling time (see Fig. 4) with a higher interfacial resistance for pellets of a smaller grain size. The electrical conductivity of BMRGO30

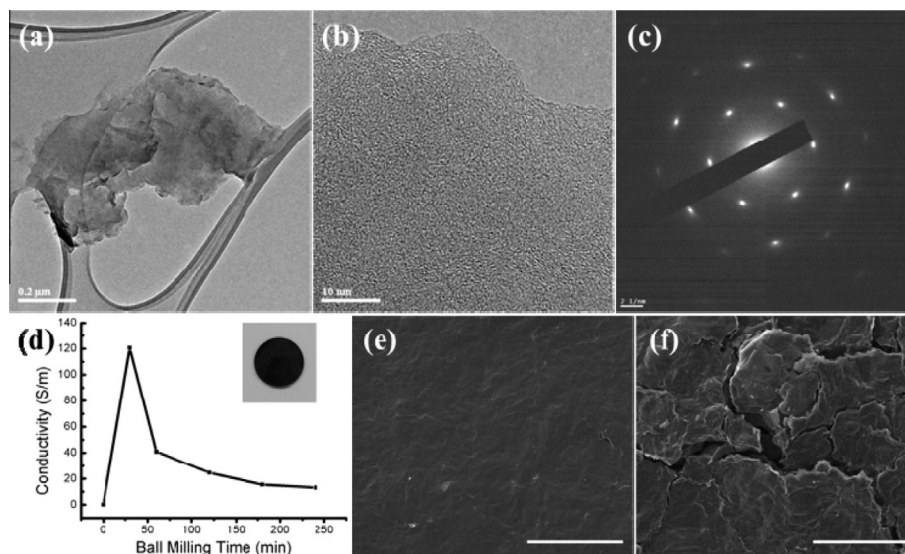


Fig. 5 – TEM Images of BMRGO30: (a) low magnification; (b) high-magnification at the edge; (c) selected area electron diffraction (SAED) pattern. (d) Conductivity plots of GO and BMRGOs with different ball-milling time. Inset is a photograph of BMRGO30 pellet with diameter of 2.5 cm used for the measurement. SEM images obtained from the surface of sample pellets after heat treatment at 900 °C for 2 h under nitrogen: (e) BMRGO30; (f) GO. Scale bars are 100 μm .

(120 S/m) is comparable to that of the RGO reduced by hydrazine [9], but much higher than that of the RGO reduced by other solution-based green approaches (Table S2). Furthermore, the post heat-treatment of BMRGO30 at 900 °C for 2 h under nitrogen can lead to additional increase in conductivity up to 3400 S/m whilst the surface of the BMRGO pellet remains intact as cohesive film with smooth surfaces (Fig. 5e). By contrast, the same thermal treatment of GO pellet makes it rough and cracked (Fig. 5f). The hygroscopic nature of GO caused the gas evolution during annealing, leading to the significant difference in thermal behaviors between GO and BMRGOs.

4. Conclusion

We have developed a solvent-free green method for the scalable production of graphene nanoplatelets (GnPs) by solid-state ball-milling of GO in the presence of hydrogen. The resultant BMRGOs show an efficient structural restoration of graphene network by elimination of various oxygenated functional groups of GO during mechanochemical ball-milling. They show also superior structural integrity with completely free from undesirable heteroatom doping. Furthermore, the resultant BMRGO pellets show electrical conductivities up to 120 and 3400 S/m before and after heat treatment (900 °C for 2 h under nitrogen), respectively. Therefore, the ball-milling technique used in this study could be regarded as an efficient general green synthetic approach toward the low-cost and high-yield production of GnPs for various applications, ranging from energy conversion through energy storage to electronic devices.

Acknowledgements

This research was supported by Mid-Career Researcher (MCR), BK21 Plus, Converging Research Center (CRC), Basic

Science Research (BSR), Basic Research Laboratory (BRL) programs through the National Research Foundation (NRF) of Korea funded by the Ministry of Education, Science and Technology (MEST), US Air Force Office of Scientific Research through Asian Office of Aerospace R&D (AFOSR-AOARD), and L.D. thanks the partial support from AFOSR (FA9550-12-1-0037).

Appendix A. Supplementary data

Supplementary data associated with this article can be found, in the online version, at <http://dx.doi.org/10.1016/j.carbon.2014.05.055>.

REFERENCES

- [1] Zhu Y, Murali S, Cai W, Li X, Suk JW, Potts JR, et al. Graphene and graphene oxide: synthesis, properties, and applications. *Adv Mater* 2010;22(35):3906–24.
- [2] Sun Y, Wu Q, Shi G. Graphene based new energy materials. *Energy Environ Sci* 2011;4(4):1113–32.
- [3] Allen MJ, Tung VC, Kaner RB. Honeycomb carbon: a review of graphene. *Chem Rev* 2010;110(1):132–45.
- [4] Novoselov KS, Geim AK, Morozov S, Jiang D, Zhang Y, Dubonos S, et al. Electric field effect in atomically thin carbon films. *Science* 2004;306(5696):666–9.
- [5] Kim KS, Zhao Y, Jang H, Lee SY, Kim JM, Kim KS, et al. Large-scale pattern growth of graphene films for stretchable transparent electrodes. *Nature* 2009;457(7230):706–10.
- [6] Choucair M, Thordarson P, Stride JA. Gram-scale production of graphene based on solvothermal synthesis and sonication. *Nat Nanotechnol* 2008;4(1):30–3.
- [7] Berger C, Song Z, Li X, Wu X, Brown N, Naud C, et al. Electronic confinement and coherence in patterned epitaxial graphene. *Science* 2006;312(5777):1191–6.

- [8] Stankovich S, Dikin DA, Dommett GH, Kohlhaas KM, Zimney EJ, Stach EA, et al. Graphene-based composite materials. *Nature* 2006;442(7100):282–6.
- [9] Stankovich S, Dikin DA, Piner RD, Kohlhaas KA, Kleinhammes A, Jia Y, et al. Synthesis of graphene-based nanosheets via chemical reduction of exfoliated graphite oxide. *Carbon* 2007;45(7):1558–65.
- [10] Dreyer DR, Park S, Bielawski CW, Ruoff RS. The chemistry of graphene oxide. *Chem Soc Rev* 2010;39(1):228–40.
- [11] Tung VC, Allen MJ, Yang Y, Kaner RB. High-throughput solution processing of large-scale graphene. *Nat Nanotechnol* 2008;4(1):25–9.
- [12] Gao W, Alemany LB, Ci L, Ajayan PM. New insights into the structure and reduction of graphite oxide. *Nat Chem* 2009;1(5):403–8.
- [13] Si Y, Samulski ET. Synthesis of water soluble graphene. *Nano Lett* 2008;8(6):1679–82.
- [14] Wang H, Maiyalagan T, Wang X. Review on recent progress in nitrogen-doped graphene: synthesis, characterization, and its potential applications. *ACS Catal* 2012;2(5):781–94.
- [15] Wang X, Li X, Zhang L, Yoon Y, Weber PK, Wang H, et al. N-doping of graphene through electrothermal reactions with ammonia. *Science* 2009;324(5928):768–71.
- [16] Guo C, Book-Newell B, Irudayaraj J. Protein-directed reduction of graphene oxide and intracellular imaging. *Chem Commun* 2011;47(47):12658–60.
- [17] Gao J, Liu F, Liu Y, Ma N, Wang Z, Zhang X. Environment-friendly method to produce graphene that employs vitamin C and amino acid. *Chem Mater* 2010;22(7):2213–8.
- [18] Chen D, Li L, Guo L. An environment-friendly preparation of reduced graphene oxide nanosheets via amino acid. *Nanotechnology* 2011;22(32):325601.
- [19] Zhu C, Guo S, Fang Y, Dong S. Reducing sugar: new functional molecules for the green synthesis of graphene nanosheets. *ACS Nano* 2010;4(4):2429–37.
- [20] Zhang J, Yang H, Shen G, Cheng P, Zhang J, Guo S. Reduction of graphene oxide vial-ascorbic acid. *Chem Commun* 2010;46(7):1112–4.
- [21] Zhou Y, Bao Q, Varghese B, Tang LAL, Tan CK, Sow CH, et al. Microstructuring of graphene oxide nanosheets using direct laser writing. *Adv Mater* 2010;22(1):67–71.
- [22] Sokolov DA, Shepperd KR, Orlando TM. Formation of graphene features from direct laser-induced reduction of graphite oxide. *J Phys Chem Lett* 2010;1(18):2633–6.
- [23] Ding Y, Zhang P, Zhuo Q, Ren H, Yang Z, Jiang Y. A green approach to the synthesis of reduced graphene oxide nanosheets under UV irradiation. *Nanotechnology* 2011;22(21):215601.
- [24] Williams G, Seger B, Kamat PV. TiO₂-graphene nanocomposites. UV-assisted photocatalytic reduction of graphene oxide. *ACS Nano* 2008;2(7):1487–91.
- [25] Guo H-L, Wang X-F, Qian Q-Y, Wang F-B, Xia X-H. A green approach to the synthesis of graphene nanosheets. *ACS Nano* 2009;3(9):2653–9.
- [26] Liao K-H, Mittal A, Bose S, Leighton C, Mkhoyan KA, Macosko CW. Aqueous only route toward graphene from graphite oxide. *ACS Nano* 2011;5(2):1253–8.
- [27] Zhu Y, Stoller MD, Cai W, Velamakanni A, Piner RD, Chen D, et al. Exfoliation of graphite oxide in propylene carbonate and thermal reduction of the resulting graphene oxide platelets. *ACS Nano* 2010;4(2):1227–33.
- [28] Zhou Y, Bao Q, Tang LAL, Zhong Y, Loh KP. Hydrothermal dehydration for the “green” reduction of exfoliated graphene oxide to graphene and demonstration of tunable optical limiting properties. *Chem Mater* 2009;21(13):2950–6.
- [29] Jeon I-Y, Shin Y-R, Sohn G-J, Choi H-J, Bae S-Y, Mahmood J, et al. Edge-carboxylated graphene nanosheets via ball milling. *Proc Natl Acad Sci USA* 2012;109(15):5588–93.
- [30] Jeon I-Y, Choi H-J, Jung S-M, Seo J-M, Kim M-J, Dai L, et al. Large-scale production of edge-selectively functionalized graphene nanoplatelets via ball milling and their use as metal-free electrocatalysts for oxygen reduction reaction. *J Am Chem Soc* 2012;135(4):1386–93.
- [31] Jeon I-Y, Choi H-J, Ju MJ, Choi IT, Lim K, Ko J, et al. Direct nitrogen fixation at the edges of graphene nanoplatelets as efficient electrocatalysts for energy conversion. *Sci Rep* 2013;3:2260.
- [32] Jeon IY, Zhang S, Zhang L, Choi HJ, Seo JM, Xia Z, et al. Edge-selectively sulfurized graphene nanoplatelets as efficient metal-free electrocatalysts for oxygen reduction reaction: the electron spin effect. *Adv Mater* 2013;25(42):6138–45.
- [33] Yan L, Lin M, Zeng C, Chen Z, Zhang S, Zhao X, et al. Electroactive and biocompatible hydroxyl-functionalized graphene by ball milling. *J Mater Chem* 2012;22(17):8367–71.
- [34] León V, Quintana M, Herrero MA, Fierro JL, de la Hoz A, Prato M, et al. Few-layer graphenes from ball-milling of graphite with melamine. *Chem Commun* 2011;47(39):10936–8.
- [35] Posudievsky OY, Khazieieva OA, Koshechko VG, Pokhodenko VD. Preparation of graphene oxide by solvent-free mechanochemical oxidation of graphite. *J Mater Chem* 2012;22(25):12465–7.
- [36] Kumar NA, Choi H-J, Shin YR, Chang DW, Dai L, Baek J-B. Polyaniline-grafted reduced graphene oxide for efficient electrochemical supercapacitors. *ACS Nano* 2012;6(2):1715–23.
- [37] Hummers Jr WS, Offeman RE. Preparation of graphitic oxide. *J Am Chem Soc* 1958;80(6):1339.
- [38] Kim T, Lee H, Kim J, Suh KS. Synthesis of phase transferable graphene sheets using ionic liquid polymers. *ACS Nano* 2010;4(3):1612–8.
- [39] Kaminska I, Das MR, Coffinier Y, Niedziolka-Jonsson J, Sobczak J, Woisel P, et al. Reduction and functionalization of graphene oxide sheets using biomimetic dopamine derivatives in one step. *ACS Appl Mater Interfaces* 2012;4(2):1016–20.
- [40] Ferrari AC, Meyer JC, Scardaci V, Casiraghi C, Lazzeri M, Mauri F, et al. Raman spectrum of graphene and graphene layers. *Phys Rev Lett* 2006;97(18):187401.
- [41] Moon IK, Lee J, Ruoff RS, Lee H. Reduced graphene oxide by chemical graphitization. *Nat Commun* 2010;1:73.
- [42] Reina A, Jia X, Ho J, Nezich D, Son H, Bulovic V, et al. Large area, few-layer graphene films on arbitrary substrates by chemical vapor deposition. *Nano Lett* 2008;9(1):30–5.